Int. J. Electrochem. Sci., 7 **(2012)** 4959 - 4973

International Journal of
ELECTROCHEMICAL
SCIENCE
www.electrochemsci.org

Synthesis, Physicochemical and Electrochemical Properties of Nickel Ferrite Spinels Obtained by Hydrothermal Method for the Oxygen Evolution Reaction (OER)

M. S. Al-Hoshan[1,3], *J. P. Singh*[2,*], *A. M. Al-Mayouf*[2,3,*], *A. A. Al-Suhybani*[2], *M. N. Shaddad*[2]

[1]Chemical Engineering Department, College of Engineering, King Saud University, Riyadh 11421, Saudi Arabia.
[2]Department of Chemistry, College of Science, King Saud University, Riyadh 11451, Saudi Arabia.
[3]The Hydrogen Energy Research Group, Sustainable Energy Technologies (SET), King Saud University, Riyadh, Saudi Arabia.
[*]E-mail: jpsbhu@yahoo.co.uk, amayouf@ksu.edu.sa

Received: 14 April 2012 / *Accepted:* 19 May 2012 / *Published:* 1 June 2012

The electrocatalysis of oxygen evolution reaction (OER) has been studied at the face centered cubic (FCC) $Ni_xFe_{3-x}O_4$ ($0 \leq x \leq 1.0$) anodes in 1M KOH solutions at 25 ^{0}C. These oxides were synthesized by the hydrothermal method and reproduced in the form of film on a nickel support by an oxide-slurry painting technique. The effect of Ni substitution in the base oxide (Fe_3O_4) was investigated with regards to morphology, structure and catalytic performance by using techniques, such as, scanning electron microscopy (SEM), infrared (IR), X-ray diffraction (XRD), cyclic voltammetry (CV), Tafel polarization, and electrochemical impedance spectroscopy (EIS). Among synthesized oxides, the NiFe2O4 electrode was found to be the most active anode for oxygen evolution (OE). Tafel slope values (b = 41±6 mV decade^{-1}) were approximately the same for each electrocatalyst in spite of the amount of the Ni-metal being doped and the order for the OER with respect to OH^- concentration were found to be ~ 2. The electrocatalytic activities of the electrodes are correlated with their surface roughness. Based on the electrode kinetic results, mechanism of the oxygen evolution is suggested.

Keywords: Nickel ferrite, Hydrothermal method, Electrocatalysis, Electrochemical properties, Oxygen evolution reaction

1. INTRODUCTION

Oxygen evolution is the basic anodic reaction of water electrolysis. As the oxygen electrode reaction possesses high activation overpotential (η) in aqueous solutions [1], intensive research has been conducted to reduce this overpotential. The essential prerequisite for the optimization of this reaction is the selection of the anode material. A variety of electrocatalysts have been investigated [1 – 6]. Among them, transition metal oxides with spinel-type (AB_2O_4; where, A & B are a bivalent & trivalent transition metal ions, respectively) and perovskite-type (ABO_3; where, A is mainly La and B = Co, Ni or Mn) structures are considered the most promising and are extensively studied [1 – 6].

Fe_3O_4 and its substituted products are potent catalytic materials for several important heterogeneously catalyzed reactions such as an anode catalysts for chlorine and chlorate production [2], synthesis of ammonia [7], decomposition of H_2O_2 [8], application in the electron transfer of hemoglobin [9], and in a biosensors [10]. As compared to Co_3O_4 [1, 3, 11, 12], these oxides have considerably higher overpotential for oxygen evolution reaction (OER) [13] and are little investigated for the electrocatalysis of OER [1, 14]. Earlier, these oxides were prepared by conventional ceramic methods [14, 15] and usually have high resistivity and low specific surface area, which thereby lead to relatively low electrocatalytic activities. In the quest to improve the specific surface area vis-à-vis the electrocatalytic properties, electrocatalysts were synthesized by adopting, mainly, two strategies; first, the development of new low temperature preparation methods [1 – 10, 16 – 20] and second, partial replacement of A or/and B sites(s) by suitable metal ions [11 – 14, 21 – 23]. Very recently, Singh et al. [23] prepared a series of Cr-substituted ferro nano-spinels (13–21 nm) using a low temperature precipitation method with a controlled pH (= 11) and found considerable enhancement in the electrocatalytic properties towards the OER. Keeping the above facts in mind, herein, we synthesized Fe_3O_4 and its Ni-substituted products by using low temperature hydrothermal method and studied their physiochemical and electrocatalytic properties towards OER in alkaline solution and results of the study are presented in this paper.

2. EXPERIMENTAL

All the reagents were of analytical grade and used without further purification. Fe_3O_4 and Ni-substituted spinellic oxides were synthesized through a simple hydrothermal process [24]. For the purpose, as per requirements for the particular oxide, ferrous ammonium sulfate (AR, BDH, 99%) and nickel sulfate (AG, E-MERCK) were mixed in a stoichiometric ratio. The solution of metal sulfates and 250 ml of 10 M NaOH solution were simultaneously poured into a Teflon-lined stainless steel autoclave (Parr Instrument Company, U.S.A., Model: 452HC2 T316) and kept at 150 ^{0}C. The sealed autoclave provides a high-temperature and high-pressure environment for the annealing of oxide. After 24 h of aging, the autoclave was cooled to room temperature and the precipitate deposited at the bottom was washed repeatedly with de-ionized (DI) water until free from SO_4^{2-} ions. The precipitate, so obtained, was dried at 80 ^{0}C in a vacuum oven over night and finally sintered at 400 ^{0}C for 8 h in an electrical furnace (Nabertherm; Germany).

Materials were characterized by recording IR spectra (NEXUS-670, FT-IR Thermo Nicolet; Thermo Scientific) and XRD (Ultima IV, X-ray diffractometer: Rigaku). In case of IR, oxide powder and purified KBr were mechanically mixed and pressed into disc shape. IR was used to analyze the changes in the surface chemical bonding and structure in the frequency range of 4000–400 cm^{-1}. The spinel-phase was confirmed via XRD using Cu-K$_\alpha$ radiation (λ = 0.15418 nm; 40 kV, 40 mA) source and the data was collected at the scan rate 0.03 deg. s^{-1}. The morphology of the oxide powders was examined using a high performance scanning electron microscope (SEM; JSM-6380LA).

Electrochemical characterizations of the materials were carried out in the form of oxide film electrode. For the purpose, slurry of the oxide-powder prepared with a few drops of Triton X-100 was painted on one side of the pretreated Ni (Aldrich, 99.9%) support, as described elsewhere [25] and subsequently heat treated in an electrical furnace at 350 ^{0}C for 2 h to obtain an adherent oxide film. The electrical contact with the oxide film was made using a crocodile clip on a small, oxide-free strip of the plate. The back of the electrode was covered with an inert nonconductive epoxy and only a single face of area 0.3 cm^2 was kept uncovered to expose with the electrolyte. The oxide loadings ranged between 2 to 3 mg cm^{-2}.

Electrochemical studies, namely, cyclic voltammograms (CV), electrochemical impedance spectra (EIS) and Tafel polarization were performed in a conventional three-electrode single compartment Pyrex glass cell using a computerized potentiostat/galvanostat (Autolab, PGSTAT30). The commercial reference and the auxiliary electrodes were Hg/HgO/1M KOH (Koslow, scientific testing instruments; Model: 5088) and pure Pt-foil, respectively. All potentials mentioned in the text are based on the Hg/HgO (E^0 = 0.098 V vs. NHE at 25 ^{0}C) electrode only. The software used for impedance, cyclic voltammetry, and Tafel polarization measurements was NOVA 1.5. The EIS of the oxide catalysts/1M KOH interface was measured over the frequency range 0.1-10^5 Hz at a potential 0.55 V, which is the region of the commencement of the OER. The double layer capacitance (C_{dl}) was analyzed using "ZSimpWin version 3.10" software.

3. RESULTS AND DISCUSSION

3.1. Physical Properties

3.1.1 Morphology of oxide powder

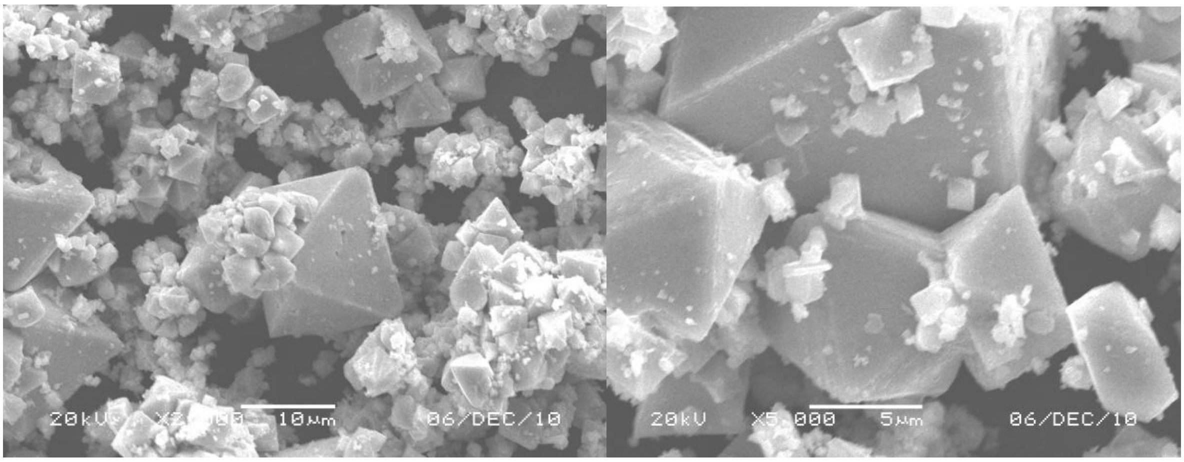

A **B**

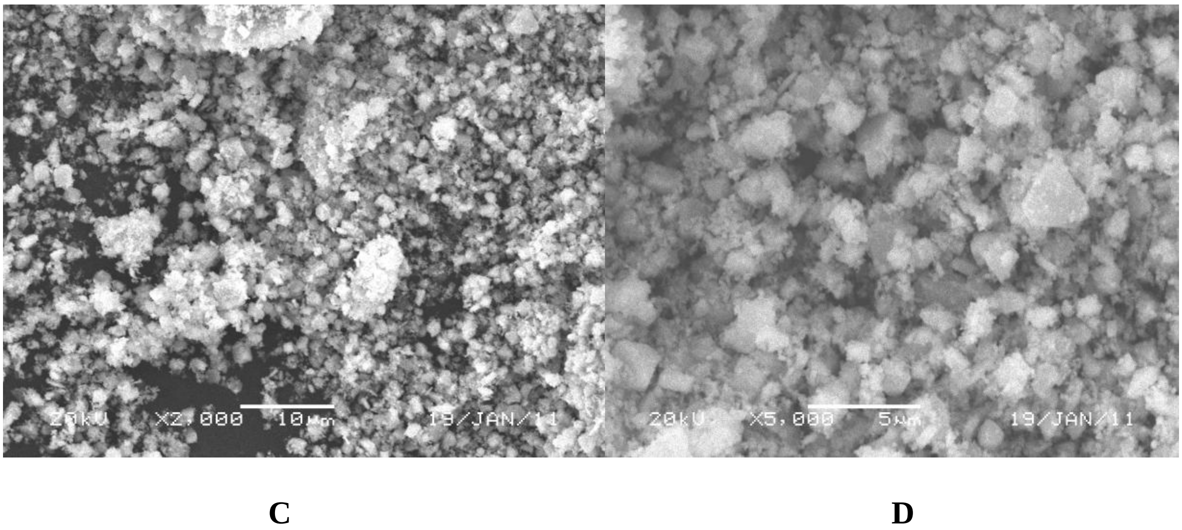

Figure 1. SEM micrographs of oxide powders; heated at 400 ^{0}C for 8 h at two magnifications: Fe_3O_4: (a) ×2,000; (b) × 5,000; $NiFe_2O_4$: (c) × 2,000; (d) ×5,000.

SEM micrographs of Fe_3O_4 and $NiFe_2O_4$ oxide powders, sintered at 400 ^{0}C for 8 h, are represented in the Fig. 1 (a & b) and Fig. 1 (c & d), respectively, at two different magnifications. From Fig. 1 (a & b), it is revealed that oxide particles have an octahedron shape with conspicuous crystal faces and inhomogeneous grain size. Some aggregates have also been observed in the morphology of Fe_3O_4 (Fig. 1a). In the case of $NiFe_2O_4$ [Fig. 1 (c & d)], the crystals are distributed more uniformly having smaller grain size. Some authors [24, 26 – 28] have also observed similar morphology on the metal oxide; highly alkalinity favors the growth of various morphologies, possibly due to the multitude of factors which influence the morphologies of the crystal grown.

3.1.2. Infrared spectra

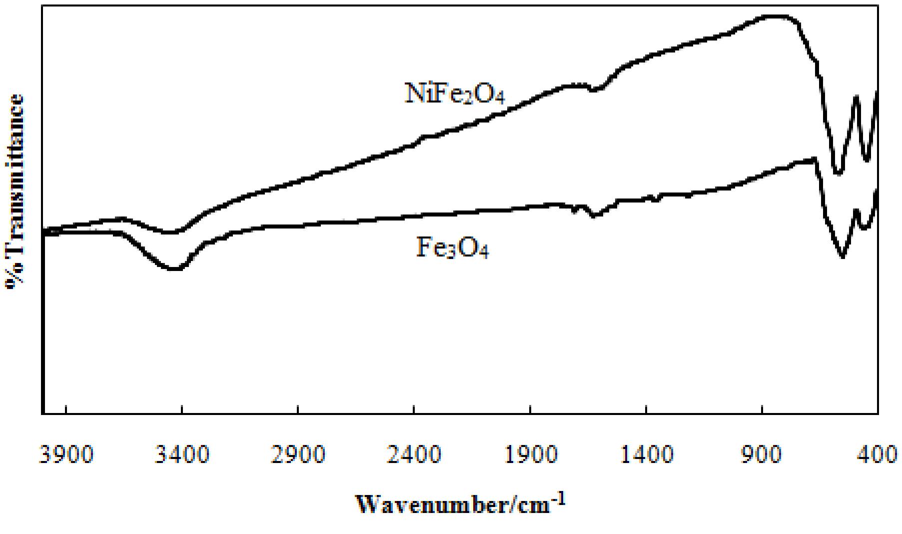

Figure 2. IR spectra of oxides; Fe_3O_4 and $NiFe_2O_4$, sintered at 400 ^{0}C for 8 h.

IR spectra for Fe_3O_4 and $NiFe_2O_4$, sintered at 400 ^{0}C for 8 h, recorded in the region of 4000-400 cm^{-1} are shown in the Fig. 2. The frequency bands (ν_1) (~ 558 & ~ 577 cm^{-1}) and (ν_2) (~ 459 & ~ 457 cm^{-1}), as shown in the figure 2, revealed the formation of pure spinel ferrites phase with two sub-lattices tetrahedral (A-site) and octahedral (B-site) sites [29 – 32]. Absorption bands ν_1 and ν_2 are attributed to the tetrahedral and octahedral site, respectively, of each oxide. The peak values ~ 3434 and ~ 3459 cm^{-1} represent the characteristic hydroxyl group (O−H) that can be attributed to the water molecule adsorbed onto the surface of Fe_3O_4 and $NiFe_2O_4$, respectively. The presence of hydroxyl group on the ferrite may help in the conjugation and dispersion of nano materials [33]. It may also help in the agglomeration of ferrite particles as the SEM images show at high resolution.

3.1.3. X-ray diffraction

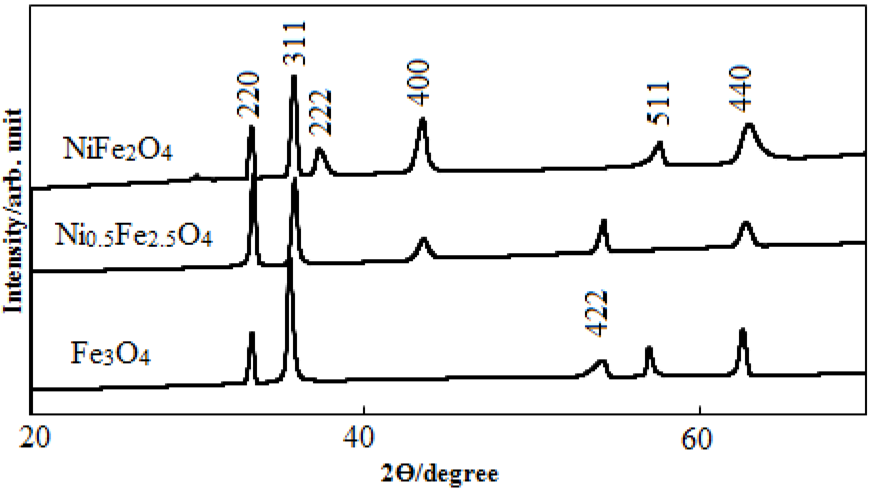

Figure 3. XRD powder patterns of Fe_3O_4, $Ni_{0.5}Fe_{2.5}O_4$ and $NiFe_2O_4$; sintered at 400 ^{0}C for 8h.

XRD patterns of Fe_3O_4 and its substituted products, recorded within the angle range of $20^0 \leq 2\theta \leq 70^0$, are shown in Fig. 3. The diffractogram exhibited X-ray lines corresponding to the spinel phase. The XRD patterns showed cubic lattice with a space group of Fd-3m for each oxide material. No additional peaks for hematite, metal hydroxides or other impurities were observed. The cell parameter 'a', of oxide powders was estimated by using the database ICDD and the results, so obtained, are shown in Table 1. It was found that the estimated values of cell parameter ‘a’ were very close to the literature values ASTM (JCPDS No. 88-0866; a = 0.8385 nm) and ASTM (JCPDS No. 44-1485; a = 0.8339 nm) for Fe_3O_4 and $NiFe_2O_4$, respectively. The a-value for 0.5 mol Ni-substituted ferrite, to our knowledge, is not reported in literature. From the data, it was observed that the cell parameter ‘a’ decreased slightly with the substitution of Ni in the base oxide. The decrease in the value of ‘a’ is, possibly, due to the difference in ionic radii of Ni^{2+} and Fe^{2+}. In $NiFe_2O_4$, the larger crystal radius Fe^{2+} (0.77 Å) is replaced by smaller ionic crystal radius Ni^{2+} (0.69 Å), which resulted the decrease in the cell parameter. The crystallite size (S) of the oxide powders was calculated from the width of the d_{311} peak by using the Scherrer equation [21]. The crystallite size of Fe_3O_4, $Ni_{0.5}Fe_{2.5}O_4$ and $NiFe_2O_4$ oxide powders were found to be ~18, ~15 and ~13 nm, respectively. The strong and sharp peaks in the XRD pattern revealed the crystalline nature of the oxide powder as also observed in the SEM observation.

Table 1. The unit cell dimensions for nickel ferrites (F. C. C. Structure)

Oxides	**Space group**	**T/ ^{0}C**	**a/ nm**	**S/ nm**
Fe_3O_4 (01-087-0246 ICDD)	Fd-3m	400	0.8391	~18
$Ni_{0.5}Fe_{2.5}O_4$ (01-087-2338 ICDD)	Fd-3m	400	0.8361	~15
$NiFe_2O_4$ (00-054-0964 ICDD)	Fd-3m	400	0.8337	~13

3.2. Electrochemical properties

3.2.1. Cyclic Voltammetry (CV)

To investigate the behavior of surface electroactive species with regard to the oxidation-reduction reaction, cyclic voltammograms (CVs) of each oxide and the bare Ni electrode were recorded in the potential region of 0.0 – 0.65 V in 1 M KOH at 25 ^{0}C at the scan rate of 20 mV s^{-1}. Typical CVs curves for the base and Ni-substituted products as well as the bare Ni electrode are shown in the Fig. 4. CVs for the each oxide electrodes were quite similar, regardless of the nature of the oxide films.

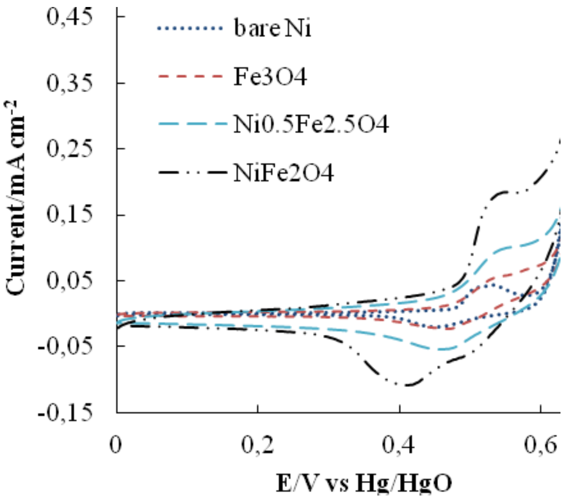

Figure 4. Cyclic voltammograms of bare Ni and $Ni_xFe_{3-x}O_4$ ($0 \leq x \leq 1.0$) ferrite electrodes on a Ni-substrate (from inner to outer; bare Ni, Fe_3O_4, $Ni_{0.5}Fe_{2.5}O_4$ and $NiFe_2O_4$, respectively) at 20 mV s^{-1} in 1M KOH at 25 ^{0}C.

Each voltammogram shown in Fig. 4 exhibited a pair of redox peaks (an anodic and a corresponding cathodic peak) prior to the onset of the OER. Values of the anodic (Ep_a) and cathodic

(Ep_c) peak potentials, the separation potential ($\Delta E = Ep_a - Ep_c$), and the formal redox potential $\{E^0 = (Ep_a + Ep_c)/2\}$ were estimated and their values, at the scan rate of 20 mV s^{-1}, are listed in Table 2. The result shows that there is appreciable increase in the ΔE values with the oxide film on Ni. However, Ni-substitution in Fe_3O_4 matrix did not influence the ΔE value. Almost, similar E^0 value is observed with each electrode, except base oxide.

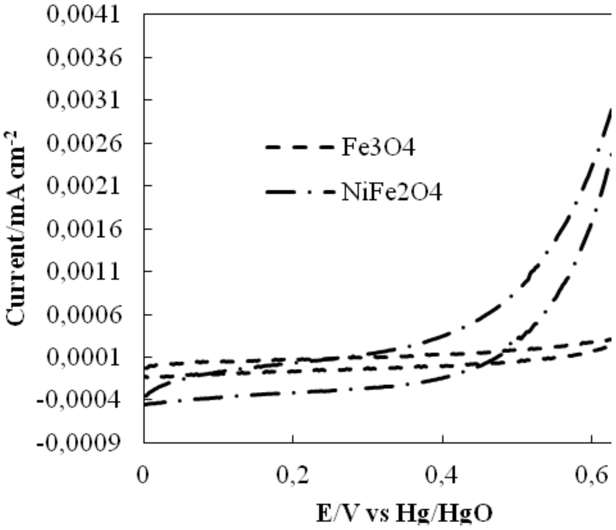

Figure 5. Cyclic voltammograms of pure ferrite (Fe_3O_4) and nickel ferrite ($NiFe_2O4$) electrodes on a Ti-substrate at 20 mV s^{-1} in 1M KOH at 25 ^{0}C.

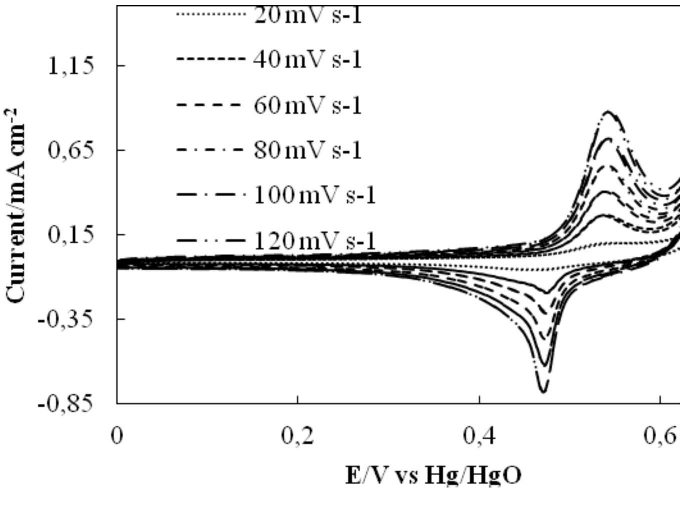

Figure 6. Cyclic voltammograms of the $Ni/Ni_{0.5}Fe_{2.5}O_4$ electrode at different scan rates (from inner to outer; 20 mV s^{-1}, 40 mV s^{-1}, 60 mV s^{-1}, 80 mV s^{-1}, 100 mV s^{-1} and 120 mV s^{-1}, respectively) in 1M KOH at 25 ^{0}C.

In order to know occurrence of redox peaks prior to the onset of OER, CV of the catalytic film on Ti was recorded under similar experimental conditions. CVs curves of Fe_3O_4 and $NiFe_2O_4$ on Ti-substrate, as shown in Fig. 5, did not give any redox peak in the potential region of 0.0 – 0.65 V. This observation and the E^0 value, shown in the Table 2, indicate that the observed redox peaks correspond to the oxidation-reduction of nickel ions from the support and not to the oxidation of ferrite films. Similar results of CVs have also been observed by some authors [11, 34 – 36]. Also, it is considered that during the experiment, the electrolyte may penetrate [37] the catalytic layer through pores, cracks, crevices, inter-crystalline gap, etc., and came in contact with the substrate and oxidize the latter. However, it does not affect the stability of the oxide film. From Table 2, it is also observed that the oxide catalyst influenced the anodic peak current density (j_{pa}) significantly. The effect is found to be greatest for the electrocatalytically most active $NiFe_2O_4$ electrode (j_{pa}= 0.17 mA cm^{-2}). This increase in the anodic peak current density might be due to the fact that the catalysts stimulate not only the oxygen evolution reaction but also the redox couple. It is thought that Ni^{2+} ions, produced at the Ni/oxide interface due to the oxidation of nickel support [18, 35] during electrolysis, influence the anodic peak current density of the catalytic films.

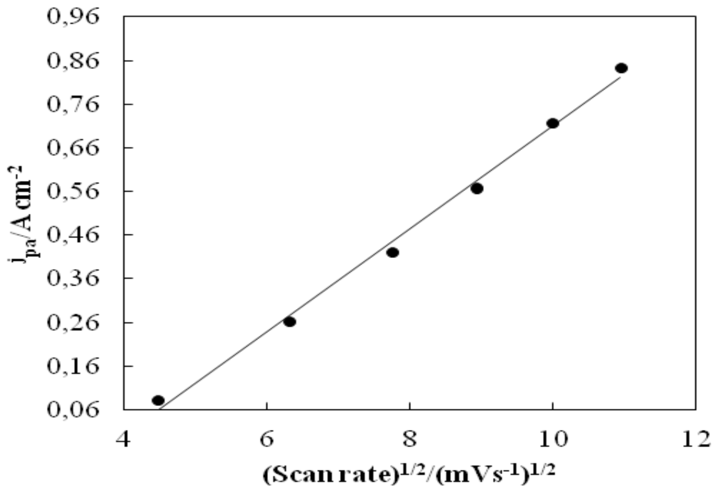

Figure 7. j_{pa} vs (scan rate)$^{1/2}$ plot for the $Ni/Ni_{0.5}Fe_{2.5}O_4$ electrode.

Table 2. Results of the cyclic voltammetry of pure and nickel ferrites in 1M KOH at 20 mV s^{-1} and 25 ^{0}C.

Electrode	Ep_a /mV	Ep_c /mV	$\Delta E=(Ep_a - Ep_c)$ /mV	$E0=(Ep_a+Ep_c)/2$ /mV	Anodic peak current density (j_{pa}) /mA cm^{-2}	Actual anodic peak current density (j_{pa})/mA cm^{-2}
Ni (bare)	505	447	58	476	0.01	-----
Fe_3O_4	581	471	110	526	0.08	0.07
$Ni_{0.5}Fe_{2.5}O_4$	540	429	111	485	0.10	0.09
$NiFe_2O_4$	530	410	120	470	0.18	0.17

To account the effect of the scan rate, CV for $Ni/Ni_{0.5}Fe_{2.5}O_4$ was recorded at different scan rate (v) and shown in Fig. 6. The plot j_{pa} vs. (v) $^{1/2}$, as shown in Fig. 7, was found to be linear, which indicates that the electrochemical reaction is controlled by a diffusion process [38].

3.2.2. Electrochemical Impedance Spectroscopy (EIS)

The EI-spectra for $Ni_xFe_{3-x}O_4$ ($0 \leq x \leq 1.0$) film on Ni and bare Ni were recorded at a constant dc potential (E = 0.55 V), in the region of commencement of oxygen evolution, in 1 M KOH at 25 ^{0}C. The nature of the spectra appeared to be similar regardless of the Ni content in the oxide film. Before recording each spectrum, the electrode was first equilibrated for 120 second at the potential 0.55 V. The representative Nyquist mode (simulated and experimental) EI-spectrum for Ni/$Ni_{0.5}Fe_{2.5}O_4$ in 1M KOH at 25 ^{0}C, shown in Fig. 8, indicated the formation of one semicircle in the entire frequency region.

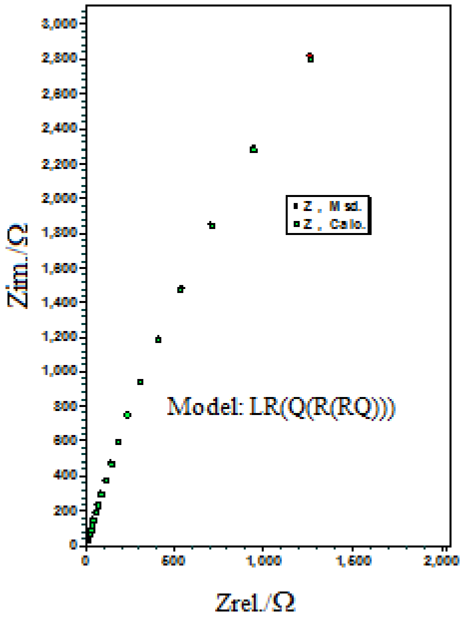

Figure 8. Nyquist plot for the Ni/$Ni_{0.5}Fe_{2.5}O_4$ electrode at E = 0.55 V in 1M KOH at 25 ^{0}C.

A single equivalent circuit, $LR_s(Q_f(R_f(R_{ct}Q_{dl})))$ was used to analyze the observed impedance response. Symbols, L, R_s, R_f, R_{ct} Q_f and Q_{dl} used to describe the circuit description code (CDC), are inductance (H), solution resistance (Ω), the oxide film (f) and charge transfer (ct) resistances in Ω, the constant phase elements (CPE) ($\Omega^{-1}s^n$) for the oxide mass and oxide catalyst/1M KOH interface, respectively. As the potentiostat introduces some inductance at high frequencies [39], the component L has been used to obtain the best fit with the experimental data. The proposed equivalent circuit model gave reasonably good fit with the experimental impedance spectra. A set of typical Bode plot (simulated and experimental) for Ni/$Ni_{0.5}Fe_{2.5}O_4$ is shown in Fig. 9 and estimates of the circuit parameters are shown in Table 3. The values of 'n', as shown in the Table 3, were found to be approximately unity regardless of the nature of the oxide film. Thus, the constant phase element (Q_{dl}) of the oxide/1M KOH interface may be considered as the total capacitance distributed along the pores of the film. Similar results have also been reported by the Singh et al. [21, 40], where the corresponding 'n' value was approximately unity.

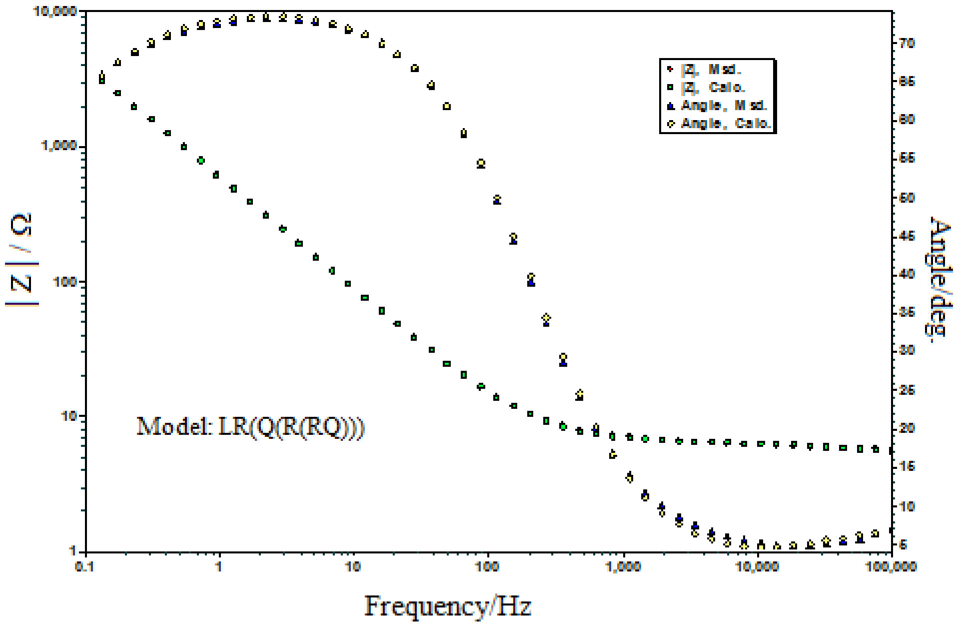

Figure 9. Bode plot for the Ni/$Ni_{0.5}Fe_{2.5}O_4$ electrode at E = 0.55 V in 1M KOH at 25 ^{0}C.

The relative values of the oxide roughness (R_F) were estimated from the ratio of the observed C_{dl} of the oxide catalyst and the C_{dl} of a smooth oxide surface (60 μF cm^{-2}) [21, 40, and 41]. The R_F values, shown in Table 3, reveal that Ni-substitution in Fe_3O_4 lattice increased the oxide roughness (R_F); the effect being greatest with 1.0 mol Ni. However, the charge transfer resistance (R_{ct}) value reduced with Ni introduction. Both R_{ct} and R_F values significantly influenced the rate of OER.

Table 3. Values of the equivalent circuit parameters for $Ni_xFe_{3-x}O_4$ ($0 \le x \le 1.0$) oxide electrodes in 1M KOH at 25 ^{0}C.

Electrodes	**10^{24} L / (H)**	**R_s /(Ω)**	**10^5 Q_f /($\Omega^{-1}sn$)**	**n_1**	**R_f /(Ω)**	**10^{-4} R_{ct} /(Ω)**	**$10^5 Q_{dl}$ / ($\Omega^{-1}s^n$)**	**n_2**	**R_F**
bare Ni	8.45	6.18	2.73	1	3.60	6.75	6.6	0.8	~1
Fe_3O_4	2221	3.12	3.64	0.6	4.71	2.63	15.7	0.9	~3
$Ni_{0.5}Fe_{2.5}O_4$	10	4.35	5.48	0.6	2.18	1.96	30.6	0.9	~5
$NiFe_2O_4$	100	3.19	19.19	0.8	2.02	1.05	41.2	0.8	~7

Similar low R_F values, obtained in the low potential region (0.0 - 0.05 V), were also reported for Ni/$Ni_xF_{3-x}O_4$ ($0.25 \le x \le 1.5$) [18], Ni/$CoFe_{2-x}Cr_xO_4$ ($0 \le x \le 1.0$) [21], Ni/$Co_xFe_{3-x}O_4$ ($0 \le x \le 1.5$), Ni/$Cu_xFe_{3-x}O_4$ ($0.1 \le x \le 1.0$) [22], Ni/$MMoO_4$ (M = Fe, Co and Ni) [25], Pt/$CoFe_{2-x}Cr_xO_4$ ($0 \le x \le 1.0$) [42] and Ni/$MnFe_{2-x}Cr_xO_4$ ($0 \le x \le 1.0$) [43]. Similar studies with ferrites seem to be scarce in the literature.

3.2.3. Electrocatalytic activity

To evaluate the electrocatalytic activity, anodic polarization curve (E vs log j), shown in Fig. 10, for the OER on each oxide film electrodes as well as bare Ni substrate were recorded at a slow scan rate of 0.2 mV s^{-1} in 1 M KOH at 25 ^{0}C.

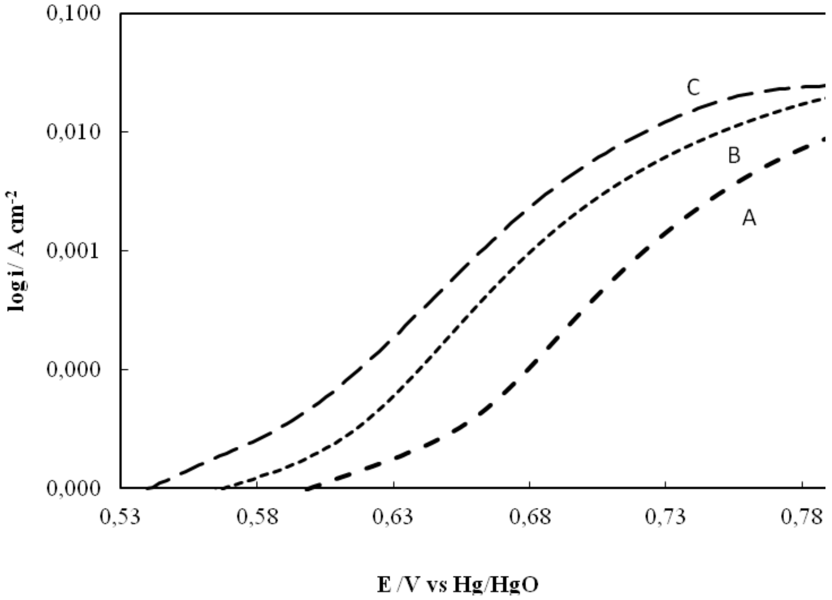

Figure 10. Tafel plots for oxygen evolution on the $Ni_xFe_{3-x}O_4$ ($0 \leq x \leq 1.0$) electrode (a): bare Ni, (b):Fe_3O_4, & (c):$NiFe_2O_4$ in 1M KOH at 25 ^{0}C (scan rate = 0.2 mV s^{-1}).

The polarization curves for each electrode were found to be almost similar, regardless of the Ni content in the base oxide. To avoid complexities/overlapping in presentation, the polarization curve for the Ni/$Ni_{0.5}Fe_{2.5}O_4$ was not shown in Fig. 10. The values of Tafel slope (b), apparent (j_a) and true ($j_t = j_a/R_F$) current densities at two different potentials (650 and 750 mV), estimated from the anodic polarization curves for oxygen evolution for each electrode, are given in the Table 4. The result showed that the OER follows almost similar mechanism on each electrode. The Tafel slope values were ranged between 35 – 47 mV decade^{-1}. In order to find out the reaction order, the Tafel polarization curve was recorded at different KOH concentrations (0.2 – 1.0 M) keeping the ionic strength ($\mu = 1.0$) of the medium constant. The ionic strength (μ) was maintained by using KNO_3 as the inert supporting electrolyte. The value of p was estimated from the slope of the plot, log j vs log C_{OH^-}, at a constant potential across the oxide film/KOH interface and found to be ~1.6, ~1.8 and ~1.9, respectively, for Fe_3O_4, $Ni_{0.5}Fe_{2.5}O_4$ and $NiFe_2O_4$. First linear region of the Tafel polarization curve was chosen for the determination of the reaction order in each case. Values of the electrode kinetic parameters (b and p) suggest that the OER on nickel ferrites follows almost the similar mechanistic path. Among the entire oxide electrode, $NiFe_2O_4$ is electrochemically the most active, while Fe_3O_4 is the least active. In terms of apparent current density (j_a) at 0.75 V, the Ni/$NiFe_2O_4$ electrode showed about 1.8 times higher activity as compared to the base oxide. However, no significant effect has been observed in the true catalytic activity. The increase in the apparent electrocatalytic activity (j_a) of the oxides with Ni content can be ascribed to an increase in the specific surface area/the roughness factor of the oxides. The consistent changing trend of R_F and catalytic activity of electrodes suggests that the electrode surface roughness plays an important role in the catalytic activity.

Based on values of the apparent current density (j_a) at E = 0.75 V in 1M KOH at 25 ^{0}C, the oxide catalysts can be arranged in the following order:

$$Fe_3O_4 < Ni_{0.5}Fe_{2.5}O_4 < NiFe_2O_4$$

Table 4. Electrode kinetic parameters for O_2 evolution on Ni/$Ni_xFe_{3-x}O_4$ ($0 \le x \le 1.0$) 1M KOH at 25 ^{0}C.

Electrodes	**Tafel slope (b) /mV decade^{-1}**	**Current (j/mA cm^{-2}) at E/mV**			
		650		750	
		j_a	j_t	j_a	j_t
bare Ni	47	0.03	0.03	3.2	3.20
Fe_3O_4	43	0.20	0.07	10.3	3.43
$Ni_{0.5}Fe_{2.5}O_4$	35	0.31	0.06	13.3	2.66
$NiFe_2O_4$	42	0.62	0.09	18.7	2.67

Most importantly, the $Ni_xFe_{3-x}O_4$ ($0 \le x \le 1.0$) electrodes prepared in this study were much more active than those of the other ferrite electrodes already reported in the literature. For instance, at $\eta_{O2} = 0.34$ V, for $NiFe_2O_4$ in 30 wt% KOH, the current density observed by Orehotsky et al. [14] was 10 mA cm^{-2}; however, our $NiFe_2O_4$ electrode gave the same current density at $\eta_{O2} \approx 0.43$ V in 1M KOH at 25 ^{0}C. The overpotential (η_{O2}) = E - E_{O2/OH^-}, where, E and E_{O2/OH^-} are the applied potential across the catalysts/1M KOH interface and the theoretical equilibrium potential in 1M KOH at 25 ^{0}C; $E_{O2/OH^-} = 0.303$ V vs Hg/HgO. At E = 0.7 V, the same electrode prepared in this study produced ~ 6 mA cm^{-2}, whereas Singh et al. [22] observed 1.2 mA cm^{-2} in 1M KOH at 25 ^{0}C for the $CuFe_2O_4$ electrode prepared by the hydroxide precipitation method at controlled pH (= 11). It was observed that the electrocatalytic activity of $NiFe_2O_4$ electrode, obtained by us, was much greater than the electrodes of other spinel magnetite family $Ni_xAl_{1-x}Mn_2O_4$ [20]. For instance, at E = 0.65 V in 1M KOH at 25 ^{0}C the apparent electrocatalytic activity of this electrode (j_a = 0.62 mA cm^{-2}) was much higher than the aluminum substituted nickel magnetites (j_a = 0.1 mA cm^{-2} at η_{O2} = 0.6V) electrodes obtained by the sol-gel as well as co-precipitation of metal hydroxides methods. However, the new electrode (E = 0.75 V at 18.7 mA cm^{-2}) showed approximately similar electrocatalytic activity to other spinel cobaltite family of Ni/$MnCo_2O_4$ electrode (η_{O2} = 0.4 V at 15 mA cm^{-2}) [44] prepared by the sol-gel route.

The observed Tafel slope (b) values (2×2.303RT/3F) were in fair agreement with those recently reported for the similar oxide electrode; $CoFe_{2-x}Cr_xO_4$ (b = 40-51 mV decade^{-1}) [21], $Ni_xFe_{3-x}O_4$ (b = ~40 mV decade^{-1}) [18], $MMoO_4$ (M = Fe, Co and Ni) (b = 37-44 mV decade^{-1}) [25], $Mn_xFe_{3-x}O_4$ (b = 36 mV decade^{-1}) [35], $MnFe_{2-x}Cr_xO_4$ (b = 34 - 41 mV decade^{-1}) [43], and $NiFe_{2-x}Cr_xO_4$ (b = 38 – 41 mV decade^{-1}) [45]. Very recently, Lyons et al. have also obtained same Tafel slopes (b = 37–47 mV decade^{-1}) on oxidized nickel, cobalt and iron electrodes in basic medium for oxygen evolution reaction [46]. A similar value for the electrode kinetic parameter (b) was also found on sprayed

$NiCo_2O_4$ film (b = 42 mV decade^{-1}), Ni [47], $CuCo_2O_4$ films (b = 42 mV decade^{-1}), Ni, $LaPO_4^-$ bonded on Ni prepared by thermal decomposition of the metal nitrates [48, 49], electrodeposited Ni-Fe alloys on mild steel (b = 37- 45 mV decade^{-1}) [50], and on austenitic stainless steels (b = 28-35 mV decade^{-1}) [36].

To account the observed electrode kinetic parameters (b and p), obtained in the present study, for oxygen evolution on spinel ferrites, the following mechanism has been proposed:

$$S + OH^- \leftrightarrow SOH + e^- \qquad (1)$$

$$SOH + OH^- \rightarrow SO + H_2O + e^- \qquad (2)$$

$$2SO \leftrightarrow 2S + O_2 \qquad (3)$$

where 'S' is an active site on the oxide surface, OH^-, and O are the surface adsorbed intermediates. This mechanism is similar to Bockris's (electrochemical oxide path) [51], Singh and coworkers [5, 22, 25, 35, 45], also Lyons et al. [46]. The possibility of other mechanisms such as Krasil'shchikov's path [52] and Bockris-Otagawa's peroxide path [41] cannot be ruled out.

At low overpotentials, considering step (2) as the rate determining and the total coverage ($\Theta_T = \Theta_{OH} + \Theta_O$) under Langmuir conditions and applying quasi-equilibrium conditions to step (1), the overall rate and hence the current density for the OER can be given as:

$$J = nFk_2k_1C^2_{OH^-} \exp [(1+\beta) FE/RT] \qquad (4)$$

k_1 is the standard equilibrium constant for reaction (1) and k_2 is the standard rate constant for reaction (2). All other symbols have their usual meanings. Assuming $\beta \sim 0.5$, equation (4) gives the second order of reaction (p) with respect to OH^- concentration and Tafel slope (b) = $2.303 \times RT/3F \approx 40$ mV decade^{-1}, which are in accordance with our experimental findings.

4. CONCLUSION

The investigation shows that the partial replacement of Fe by Ni in the Fe_3O_4 spinel lattice greatly enhances the apparent electrocatalytic activity of the oxide toward the OER. The oxide, $NiFe_2O_4$, indicated approximately 1.8 times more catalytic activity and ≈ 2.5 times more roughness than base oxide (Fe_3O_4) in 1M KOH at 25 ^{0}C.

ACKNOWLEDGEMENTS
The authors are grateful to Dr. N. K. Singh, Department of Chemistry of Lucknow University, India for reading the manuscript, correction of the written English and for his useful suggestions.

References

1. E.J.M. O’Sullivan, E.J. Calvo (1987) In: *R.G. Compton (ed) Comprehensive chemical kinetics*, vol. 27. Elsevier, Amsterdam, pp 247.
2. S. Trasatti, G. Lodi (1981) In: *S. Trasatti (ed) Electrodes of conductive metallic oxides, part B*, Elsevier, Amsterdam, pp 521.
3. S. Trasatti (1994) In: *J. Lipkowski, P.N. Ross (eds) Electrochemistry of novel materials.* VCH, New York, pp 207.
4. S.K. Tiwari, S.P. Singh, R.N. Singh, *J. Electrochem. Soc.* 143 (1996) 1505.
5. B. Lal, N.K. Singh, S. Samuel, R.N. Singh, *J. New Mater. Electrochem. Systems* 2 (1999) 59.
6. M. Hamdani, R.N. Singh, P. Chartier, *Int. J. Electrochem. Sci.* 5 (2010) 556.
7. R.R. Rajaram, A. Sermon, *J. Chem. Soc. Faraday Trans.* 81 (1985) 2577.
8. C.B. Roy, *J. Catal.* 12 (1968) 29.
9. G. Zhao, J.-J. Xu, H.-Y. Chen, *Electrochem. Commun.* 8 (2006) 48.
10. K.S. Loh, Y.H. Lee, A. Musa, A.-A. Salmah, I. Zamri, *Sensors* 8 (2008) 775.
11. F. Svegl, B. Orel, I. Grabec-Svegl, V. Kaucic, *Electrochim. Acta* 45 (2000) 4359.
12. E. Rios, P. Chartier, J.-L. Gautier, *Solid State Sci.* 1 (1999) 267.
13. P.D. Allen, N.A. Hampson, G.J. Bignold, *J. Electroanal. Chem.* 99 (1979) 299.
14. J. Orehotsky, H. Huang, C.R. Davidson, S. Srinivasan, *J. Electroanal. Chem.* 95 (1979) 233.
15. I. Nikolov, R. Darkaou, E. Zhechevo, R. Stayanova, N. Dimitrov, T. Vitanov, *J. Electroanal. Chem.* 429 (1997) 157.
16. E. Rios, J.-L. Gautier, G. Poillerat, P. Chartier, *Electrochim. Acta* 44 (1998) 491.
17. S. Ayyappan, J. Philip, B. Raj, *Mater. Chem. Phy.* 115 (2009) 712.
18. N.K. Singh, R.N. Singh, *Ind. J. Chem.* 38 (1999) 491.
19. D. Peng, S. Beysen, Q. Li, J. Jian, Y. Sun, J. Jiwuer, *Particuology* 7 (2009) 35.
20. J. Ponce, J.-L. Rehspringer, G Poillerat, J.-L. Gautier, *Electrochim, Acta* 46 (2001) 3373.
21. R.N. Singh, N.K. Singh, J.P. Singh, *Electrochim. Acta* 47 (2002) 3873.
22. J.P. Singh, N.K. Singh, R.N. Singh, *Int. J. Hydrogen Energy* 24 (1999) 433.
23. R.N. Singh, J.P. Singh, B. Lal, A. Singh, *Int. J. Hydrogen Energy* 32 (2007) 11.
24. B. Mao, Z. Kang, E. Wang, S. Lian, L. Gao, C. Tian, C. Wang, *Mater. Res. Bull.* 41 (2006) 2226.
25. R.N. Singh, J.P. Singh, A. Singh, *Int. J. Hydrogen Energy* 33 (2008) 4260.
26. W.J. Zheng, W.Q. Pang, G.Y. Meng, D.K. Peng, *J. Mater. Chem.* 9 (1999) 2833.
27. S.Y. Lian, E.B. Wang, L. Gao, Z.H. Kang, D. Wu, Y. Lan, L. Xu, *Solid State Commun.* 132 (2004) 375.
28. X.M. Liu, S.Y. Fu, H.M. Xiao, *Mater. Lett.* 60 (2006) 2979.
29. S.A. Patil, V.C. Mahajan, A.K. Ghatage, S.D. Lotke, *Mater. Chem. Phys.* 57 (1998) 86.
30. Z. J. Zhang, X. Y. Chen, B. N. Wang, C. W. Shi, *J. Crystal Growth* 310 (2008) 5453.
31. L. G. She, L. L. Ping, R. L. Smith Jr., H. Inomata, *J. Mol. Stuct.*560 (2001) 87.
32. A. Pradeep, P. Priyadharsini, G. Chandrasekaran, *Mater. Chem. Phys.* 112 (2009) 572.
33. B. Dong, B.L. He, Y.M. Chai, C.G. Liu, *Mater. Chem. Phys.* 120 (2010) 404.
34. X. Wang, H. Luo, H. Yang, P.J. Sebastian, S.A. Gamboa, *Int. J. Hydrogen Energy* 29 (2004) 967.
35. N.K. Singh, S.K. Tiwari, K.L. Anitha, R.N. Singh, *J. Chem. Soc. Faraday Trans.* 92 (1996) 2397.
36. S.K. Tiwari, K.L. Anitha, R.N. Singh, *J. Electroanal. Chem.* 319 (1991) 263.
37. C. Iwakura, A. Honji, H. Tamura, *Electrochim. Acta* 26 (1981) 1319.
38. J.P. Singh, X.G. Zhang, H.-L. Li, A. Singh, R.N. Singh, *Int. J. Electrochem. Sci.* 3 (2008) 416.
39. B.A. Boukamp, *Solid State Ionics* 20 (1986) 31.
40. R.N. Singh, B. Lal, M. Malviya, *Electrochim. Acta* 49 (2004) 4605.
41. J.O.M. Bockris, T. Otagawa, *J. Electrochem. Soc.* 131 (1984) 290.
42. R.N. Singh, N.K. Singh, J.P. Singh, G. Balaji, N.S. Gajbhiye, *Int. J. Hydrogen Energy* 31 (2006) 701.

43. R.N. Singh, J.P. Singh, H.N. Cong, P. Chartier, *Int. J. Hydrogen Energy 31* (2006) 1372.
44. J.P. Singh, R.N. Singh, *Ind. J. Chem. 39A* (2000) 819.
45. R.N. Singh, J.P. Singh, B. Lal, M.J.K. Thomas, S. Bera, *Electrochim. Acta* 51 (2006) 5515.
46. M.E.G. Lyons, M.P. Brandon, *J. Electroanal. Chem.* 641 (2010) 119.
47. S.K. Tiwari, S. Samuel, R.N. Singh, G. Poillerat, J.-F. Koenig, P. Chartier, *Int. J. Hydrogen Energy* 20 (1995) 9.
48. N. Fradette, B. Marsan, *J. Electrochem. Soc.* 145 (1998) 2320.
49. K. Fatih, B. Marsan, *Can. J. Chem.* 75 (1997) 1597.
50. R.N. Singh, J.P. Pandey, K.L. Anitha, *Int. J. Hydrogen Energy* 18 (1993) 467.
51. J.O.M. Bockris, T. Otagawa, *J. Phys. Chem.* 87 (1983) 2960.
52. A.I. Krasil'schikov, *Zh Foziche Khim* 37 (1963) 531.

© 2012 by ESG (www.electrochemsci.org)